Supplementary information for

In situ EXAFS study of Sr adsorption on TiO_2(110) under high ionic strength wastewater conditions

Arjen van Veelen[±$], Paul C. M. Francisco[ƒ], Nicholas P. Edwards[±], J. Frederick W. Mosselmans[‡], Tsutomu Sato[ƒ] and Roy A. Wogelius[±*]*

[±]Williamson Research Centre, School of Earth and Environmental Sciences, University of Manchester, Oxford Road, Manchester, M13 9PL, United Kingdom
[$]Material Science and Technology Division, Los Alamos National Laboratory, Los Alamos, NM 87545, United States
[ƒ]Laboratory of Environmental Geology, Faculty of Engineering, Hokkaido University, Kita 13 Nishi 8, Kita-ku, 060-8628 Sapporo, Japan
[‡]Diamond Light Source, Harwell Science and Innovation Campus, Fermi Avenue, Didcot, OX11 0DE, United Kingdom

TABLE OF CONTENT **page**

Table S1. Full experimental conditions of all experiments performed.

Experiment	m (g)	V (mL)	Surface area (m^2)	[Sr] (ppm)	Time (h)	[CO_3] (mM)	[Cl] (M)	ads. Sr (µg)
Powder $SrCl_2$								
adsorption isotherm	0.5	20	18.395	0, 0.5, 50, 100, 250, 500, 1000	48		0.25	
adsorption rate	0.5	20	18.395	100	0, 0.25, 0.5, 1, 2, 4, 8, 24, 48		0.25	
carbonate effect	0.5	20	18.395	100	24	0, 0.05, 0.1, 0.25, 0.5, 1, 2.5, 5	0.25	
Powder $SrCO_3$								
adsorption rate	0.25	20	9.198	50	0, 0.25, 0.5, 1, 2, 4, 8, 24, 48	0.6	0.25	
chlorine effect	0.25	20	9.198	50	24	0.6	0, 0.05, 0.15, 0.25	
EXAFS rutile(110)								
Ex situ $SrCl_2$		5	2x10-4	500	48		0.25	251.35
Ex situ $SrCO_3$		5	2x10-4	50	48		0.25	196.35
In situ $SrCl_2$		~7.9	1x10-4	500	3.7		0.25	43.24

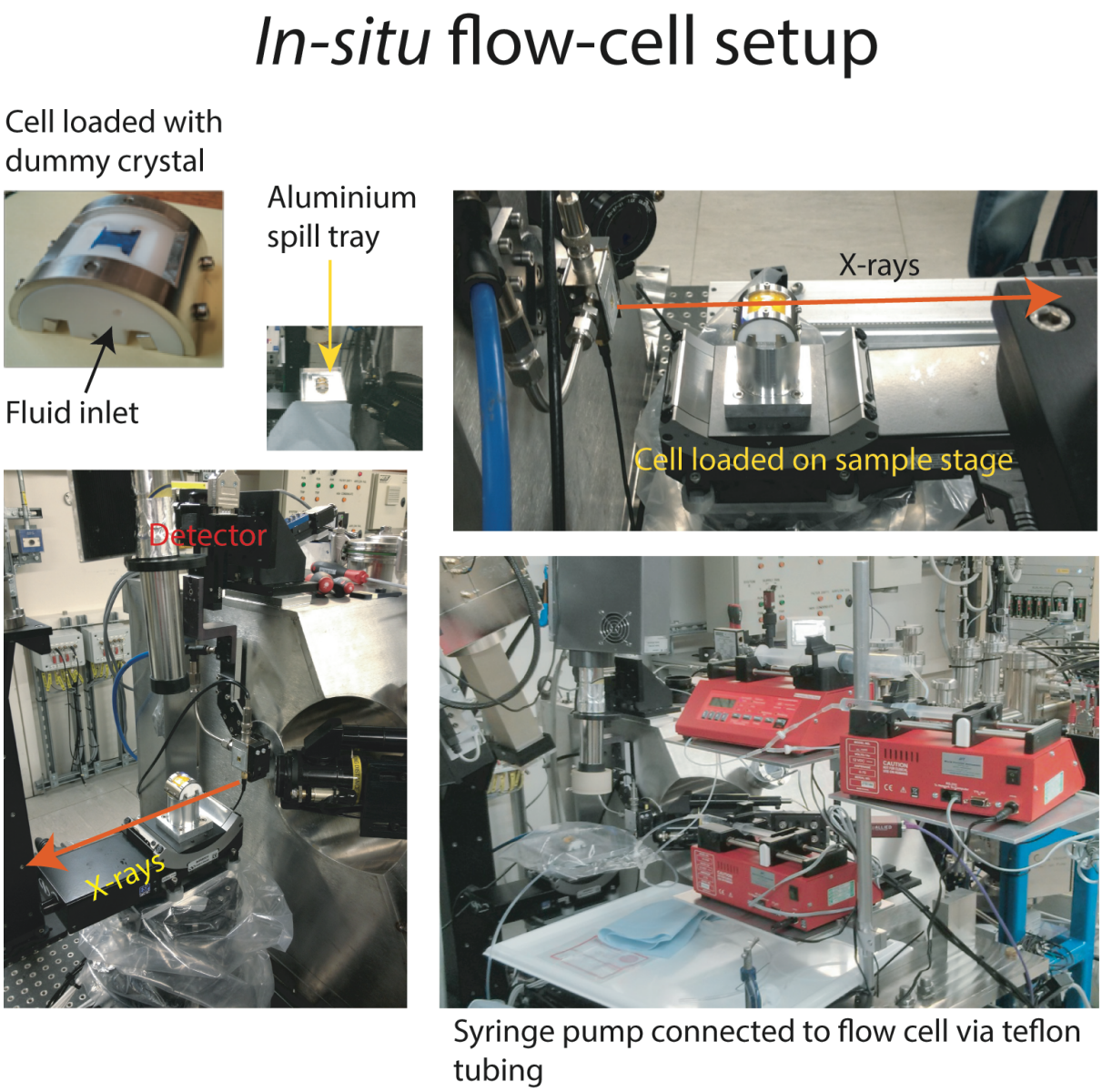

Figure S1. *In situ* flow-cell setup at the beamline I18 at Diamond Light Source.

Table S2. Batch bulk adsorption and synchrotron *in-situ* adsorption experimental fitting results.

Fitting model	Langmuir		Adsorption rate			
Experiment			1st order		2nd order	
Powder SrCl2						
Adsorption isotherm	K_L	0.0074				
	q_m	2.172				
	r^2	0.995				
Adsorption rate			K	0.052	k_2	0.14
			q_e	0.543	q_{e2}	0.572
			r^2	0.987	r^2	0.988
Carbonate effect	K_L	0.342				
	q_m	3.148				
	r^2	0.994				
Powder SrCO3						
Adsorption rate			K	0.06	k_2	0.08
			q_e	1.359	q_{e2}	1.408
			r^2	0.977	r^2	0.943
Chlorine effect	K_L	0.034				
	q_m	1.499				
	r^2	0.757				
EXAFS in situ rutile(110)						
First adsorption reaction			K	1.893	k_2	5.796
			q_e	0.947	q_{e2}	0.97
			r^2	0.996	r^2	0.952
Second adsorption reaction			K	2.448	k_2	7.72
			q_e	0.885	q_{e2}	1.021
			r^2	0.985	r^2	0.999

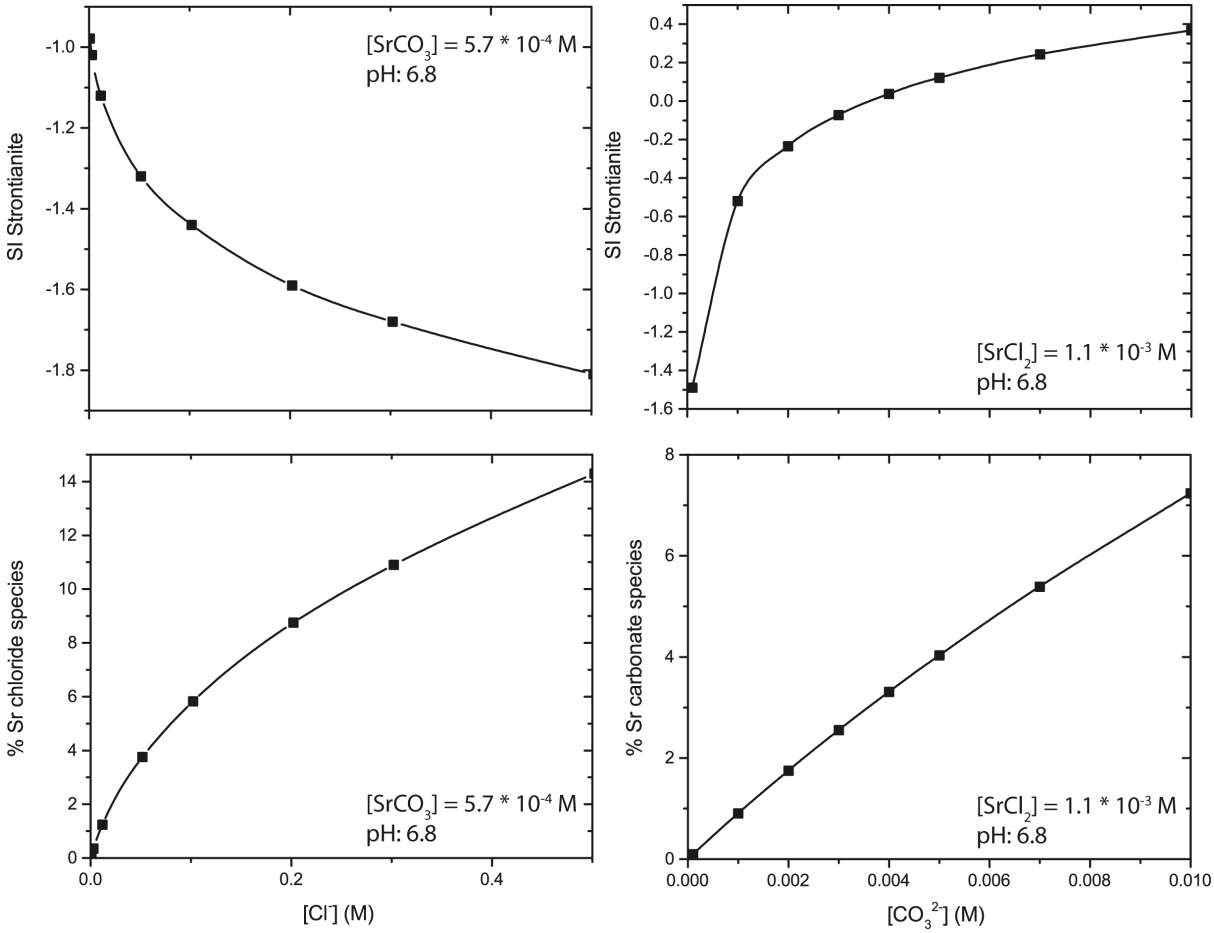

Figure S2. Sr species modeling using PHREEQC (SIT database). Left top, saturation indices of strontianite ($SrCO_3$) versus [Cl^-]. Right top, saturation indices of strontianite versus [CO_3^{2-}]. Left bottom, percentage $SrCl^+$ species of total Sr^{2+} versus [Cl^-], and right bottom, percentage Sr-carbonate species (predominantly $SrHCO_3^+$) of total Sr^{2+} versus [CO_3^{2-}].

Table S3. X-ray reflectivity fitting results of adsorbed Sr on rutile(110)

Sample	Layer	Thickness		Roughness		Density		χ^2
		(Å)	(±)	(Å)	(±)	(g cm^{-3})	(±)	
Unreacted Rutile	Water	13.80	1.85	2.88	2.55	0.948	0.179	3.75E-04
	Rutile Surface			2.09	0.93			
Ex-Situ Reacted Rutile with $SrCl_2$	$SrCl_2$ $2H_2O$ Am	17.07	3.14	1.40	0.77	2.120	0.084	8.27E-04
	Rutile			3.12	1.44			
In-Situ Reacted Rutile with $SrCl_2$	$SrCl_2$ $2H_2O$ Am	20.69	0.44	1.46	0.32	3.065	0.048	5.16E-04
	Rutile Surface			3.95	0.66			
Ex-Situ Reacted Rutile with $SrCO_3$	SrCO3	14.49	2.57	3.02	0.87	3.135	0.184	9.05E-04
	Rutile surface			2.60	1.79			

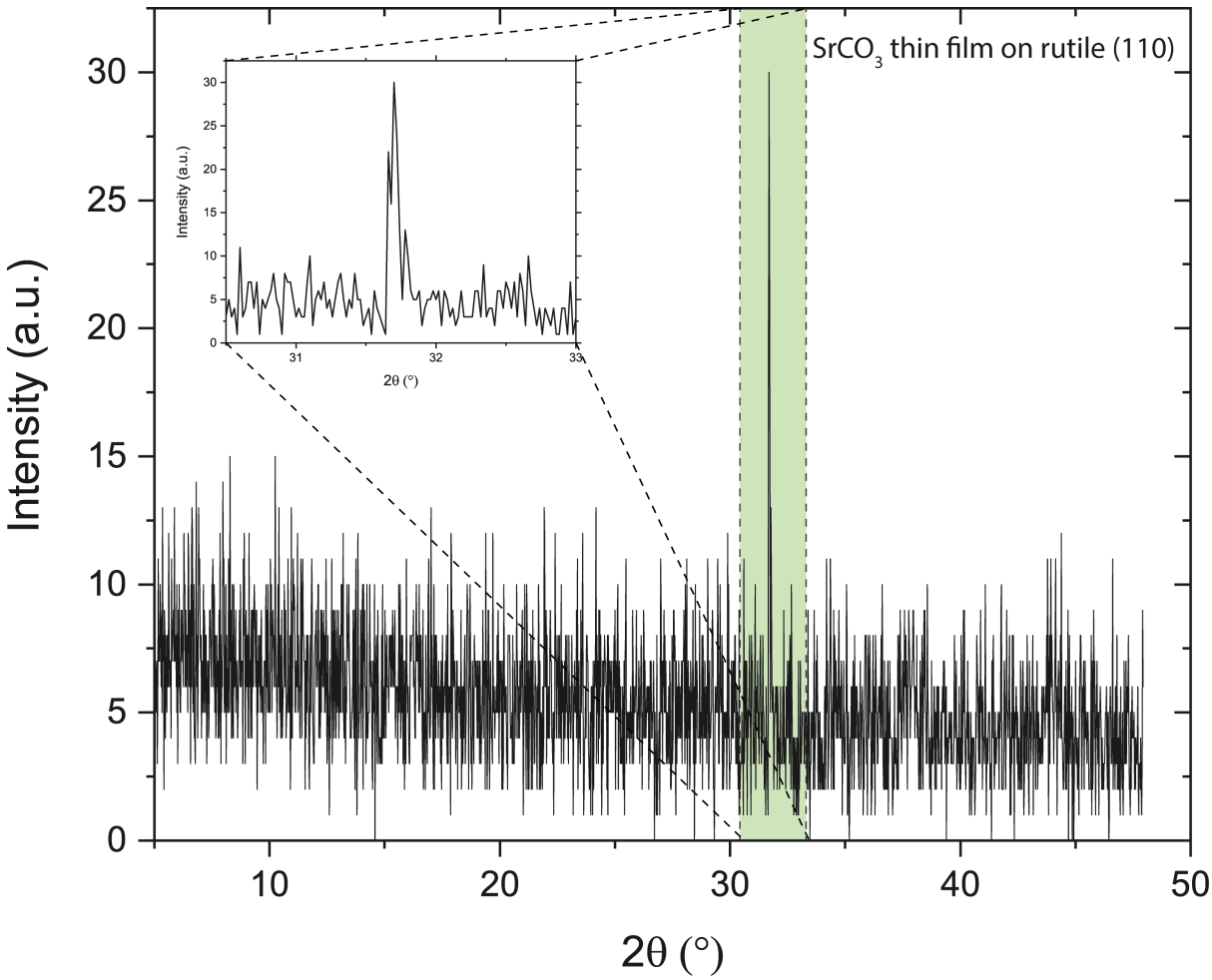

Figure S3. Grazing incidence XRD pattern of $SrCO_3$ adsorbed to the rutile(110) surface. The sharp and thin FHWM of the Bragg peak indicates that this is a rather organized surface precipitate with a d-spacing of 2.823 Å.

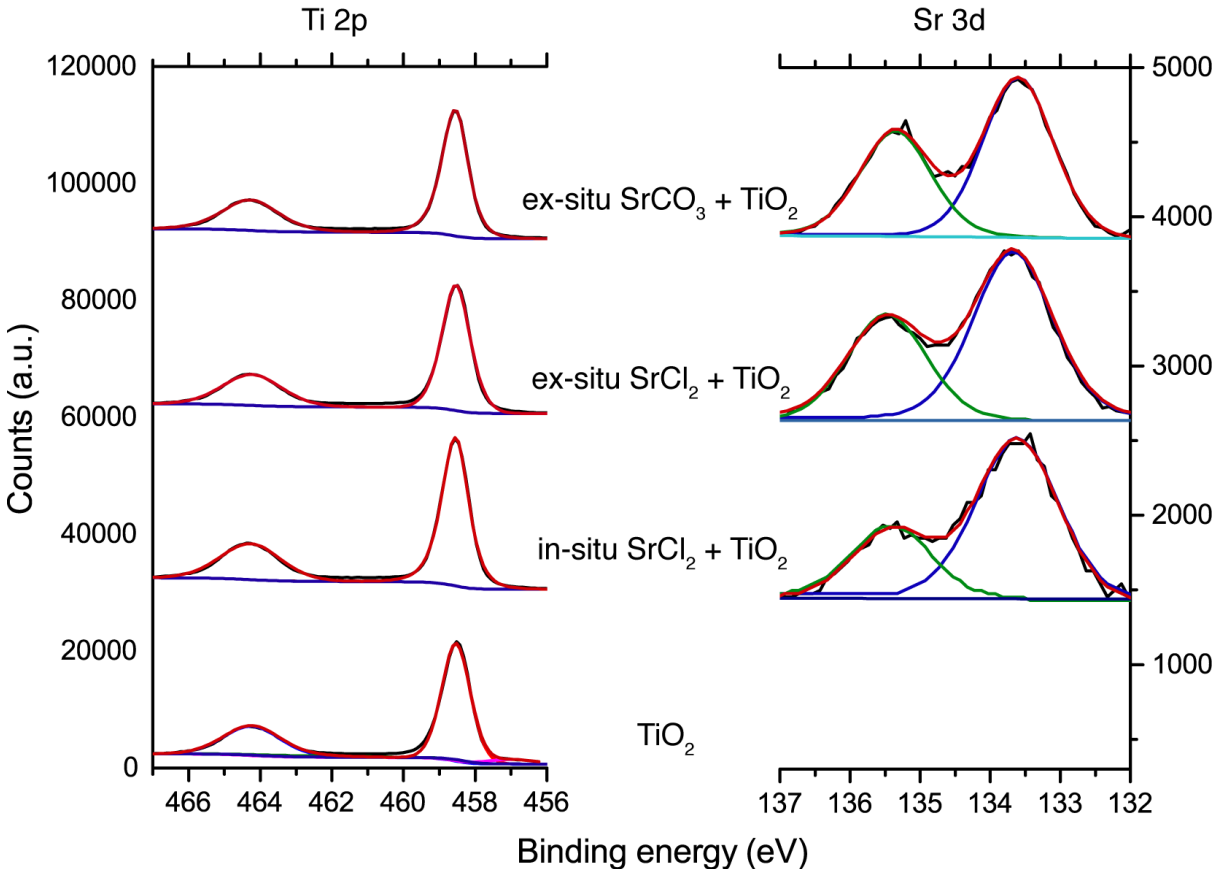

Figure S4. Ti 2p and Sr 3d measured XPS spectra. X-ray source was an Al Kα set at 1486.7 eV with pass energy of 20 eV and chamber pressure of 3 – 4 x 10^{-9} bar. The spectra were calibrated using the C 1s peak of adventitious carbon, defined at 284.8 eV.

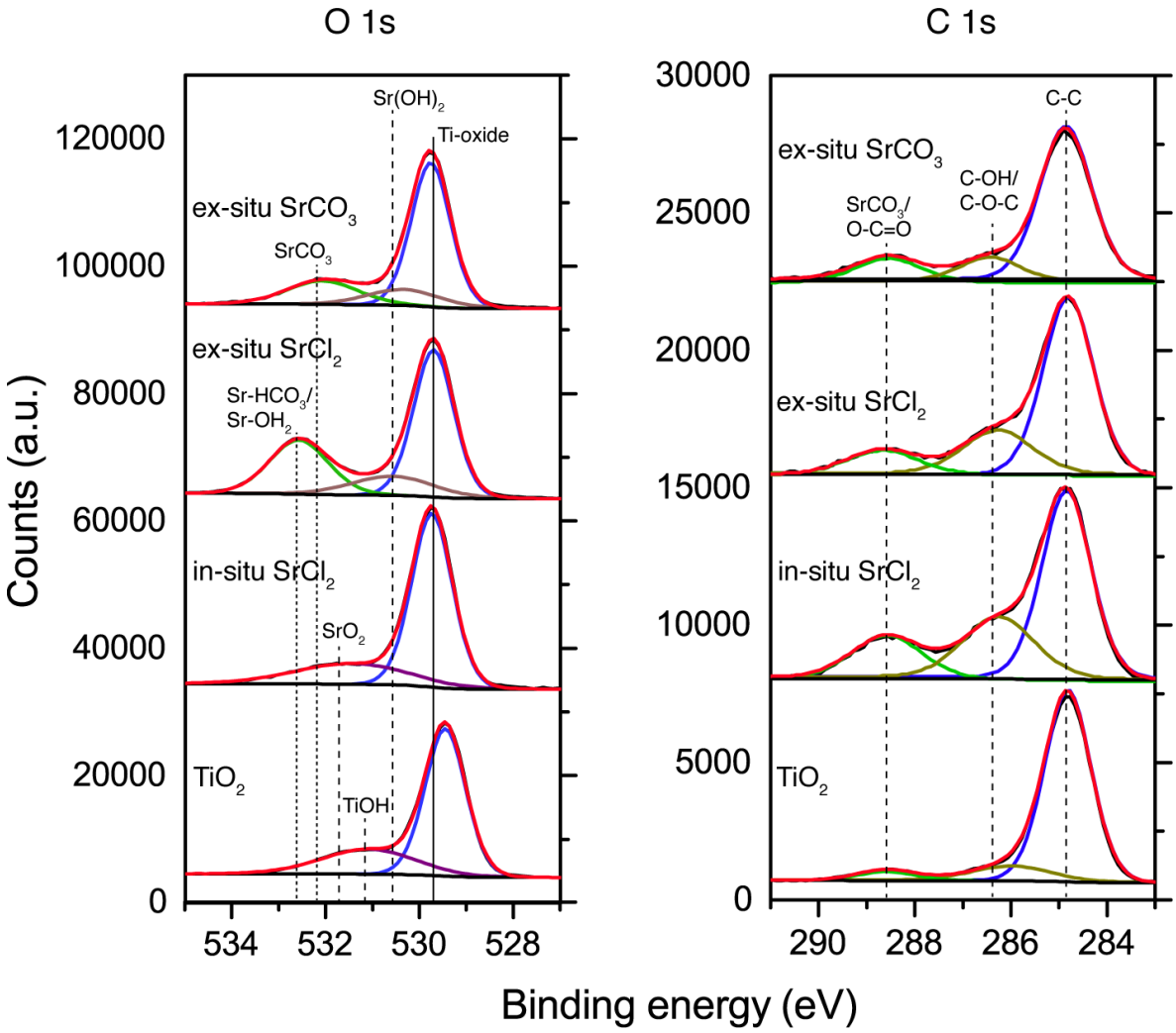

Figure S5. O 1s and C 1s measured XPS spectra. X-ray source was an Al Kα set at 1486.7 eV with pass energy of 20 eV and chamber pressure of 3 – 4 x 10^{-9} bar. The spectra were calibrated using the C 1s peak of adventitious carbon, defined at 284.8 eV.

Table S4. XPS fitting results of Sr, O, Ti and C under the four conditions.

	Sr 3d	BE* (eV)	Δ BE	O 1s	BE (eV)	%[$]	Ti 2p	BE (eV)	Δ BE	C 1s	BE (eV)	%
TiO_2(110) unreacted				lattice oxide	529.45	71.9	2p (3/2)	458.27		C-C	284.81	81.9
				hydrated	531.09	28.1	2p (1/2)	463.98	5.71	C-O-C/C-O	285.99	12.1
				Residual	4.80		Residual	23.91		O-C=O	288.59	6.0
										Residual	2.06	
TiO_2 (110) + $SrCO_3$	3d (5/2)	133.60		lattice oxide	529.76	66.5	2p (3/2)	458.57		C-C	284.86	73.3
	3d (3/2)	135.35	1.75	$Sr(OH)_2$	530.33	13.9	2p (1/2)	464.29	5.72	C-O-C/Sr-C-O	286.44	12.2
	Residual	0.89		$SrCO_3$	532.08	19.7	Residual	8.34		O-C=O/$SrCO_3$	288.54	14.5
				Residual	1.56					Residual	0.86	
TiO_2 (110) + $SrCl_2$	3d (5/2)	133.61		lattice oxide	529.74	75.0	2p (3/2)	458.55		C-C	284.84	56.3
	3d (3/2)	135.41	1.8	SrO_2	531.46	25.0	2p (1/2)	464.27	5.72	C-O-C/Sr-C-O	286.26	25.5
	Residual	0.76		Residual	1.94		Residual	7.35		O-C=O/SrCO3	288.58	18.2
										Residual	1.00	
ex-situ $SrCl_2$	3d (5/2)	133.69		lattice oxide	529.70	55.4	2p (3/2)	458.54		C-C	284.80	64.1
	3d (3/2)	135.49	1.8	$Sr(OH)_2$	530.58	14.9	2p (1/2)	464.24	5.71	C-O-C/Sr-C-O	286.27	22.9
	Residual	0.85		$SrCO_3$/$SrHCO_3^-$	532.58	29.8	Residual	14.51		O-C=O/$SrCO_3$	288.67	13.0
				Residual	2.58					Residual	1.10	

* BE—Binding energy (eV), [$] %—percentage of species of the total measured elemental spectrum

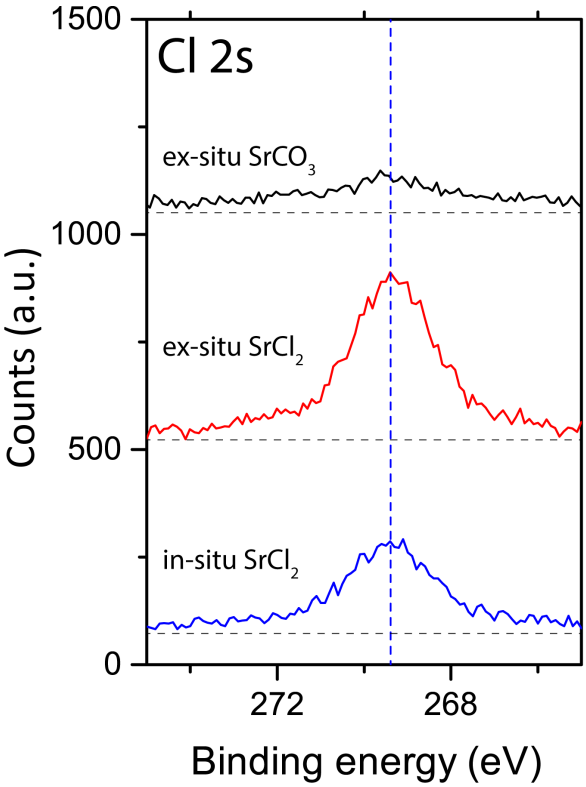

Figure S6. Cl 2s measured XPS spectra. Instruments settings are the same as for figure S3 and S4.

SS1. EXAFS fitting routine Sr EXAFS

Table S5. Extracted path lengths from crystallographic data from the literature.

Shell	**CN**	**R**	**CN**	**R**	**CN**	**R**	**CN**	**R**
	$SrCO_3$ (aragonite structure)[1]		*$Sr(OH)_2$*[2]		*$SrCl_2 \cdot 6H_2O$*[3]		*$SrCl_2 \cdot 4H_2O$*[4]	
Sr-O	1	2.5647	1	2.495	3	2.562	1	2.561
Sr-O	2	2.5780	2	2.554	6	2.709	1	2.642
Sr-O	2	2.6401	2	2.578			1	2.669
Sr-O	2	2.6515	1	2.657			1	2.673
Sr-O	2	2.7298	1	2.768			1	2.677
Sr-O							1	2.685
Sr-O							1	2.692
Sr-O							1	2.707
Sr-O							1	2.712

From the table it can be observed that in virtually any Sr bearing mineral the Sr-O varies a lot. Some less than others. Variation from ~0.08 – 0.1 is significant and can be easily captured with EXAFS. Distances less than 0.02 are likely not significant to be fitted accurately, and therefore combined. For that we will need much better data, and probably collected at a temperature where the Debye-Waller curve is plateaued out (usually around 60-80 K) and even then, this will probably be difficult, especially when there are many varying Sr-O distances. However, we need to state here that this discussion is about **crystalline phases, with crystallographic ordering.** Since we are dealing with thin films, the coordination environment is likely to be different, but we would not expect all oxygen distances to be identical in the first shell.

From this basis we started fitting our samples. Each sample condition was different enough to expect subtle differences in speciation. For our fitting model we also used chemical reasonableness, in other words if it makes sense. For example, in our *ex situ* system which was dried we observed a XANES spectrum that has similarities with our $SrCl_2$:$6H_2O$ spectrum. Therefore, it is reasonable to assume that Cl might be in the structure.

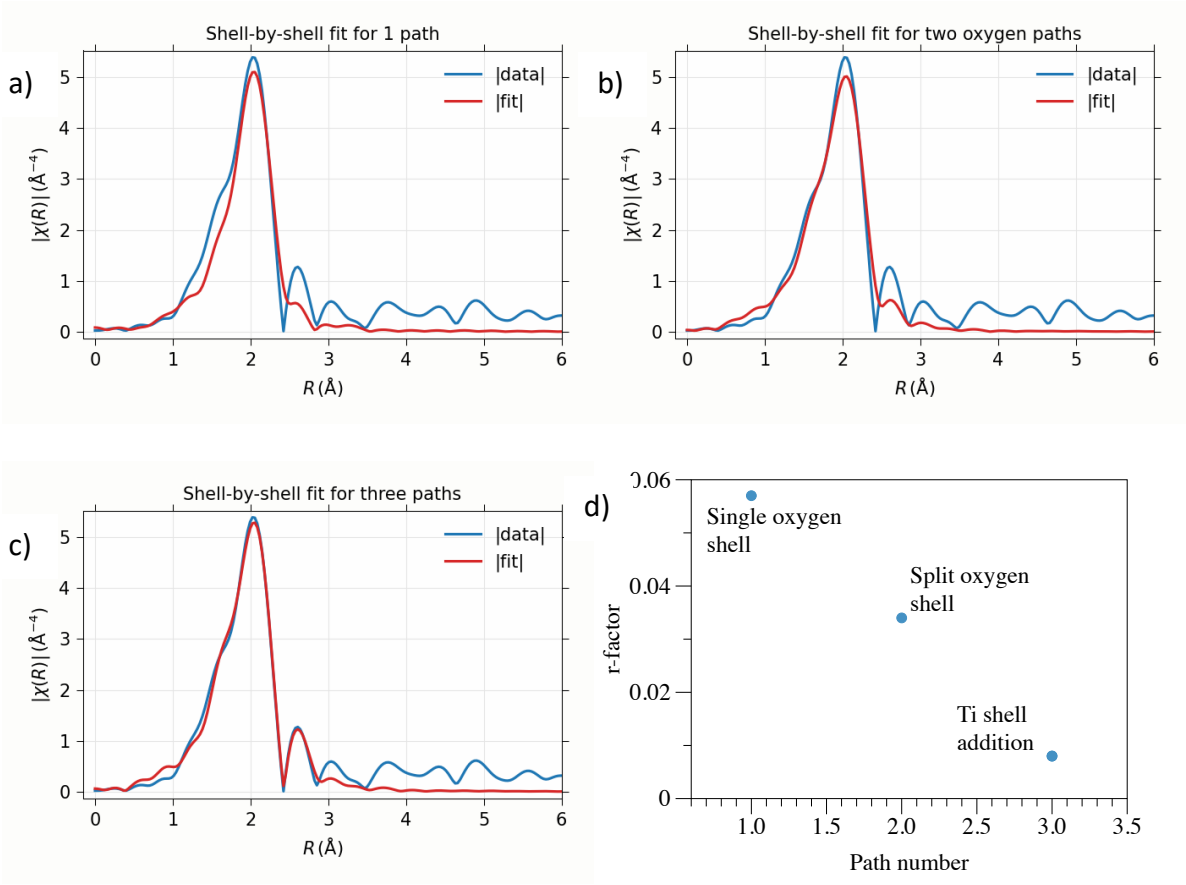

Figure S7. Fitting routine of a) one shell with oxygen atins, which clearly shows that one shell is not sufficient, b) same fit, but applying a split shell of oxygen atoms. The addition of a Ti shell in c) improved the fit even further. Figure 1d shows how the fitting quality improved adding the shells in a-c.

Figure 1a shows the fitting routine of 9 oxygen atoms in the first shell. We obtained results and can see that there is a parameter missing. We applied the split shell and kept the number of oxygen atoms the same, but split over two shells (Figure 1b). Our fit improved. Then we fitted Ti, and our fit drastically improved (Figure 1c). We also did a fit where we included Ti and one shell of oxygen atoms, but the fit was significantly worse.

SS2. Polarization dependence *ex situ* $SrCO_3$

To go into detail about the fit, we first need to understand the sample. In this particular sample we found a surface precipitate that was characterized as a thin film of $SrCO_3$ polymerized on the crystal surface. Our GI-XRD results gave a heavy textured diffraction pattern, suggesting an oriented periodic film. When comparing the EXAFS of $SrCO_3$ and the *ex situ* $SrCO_3$, we can observe an increase in amplitude between k 6 – 9 $Å^{-1}$. The likely reason for this can be explained by some form of an organized layer that as a result will create a polarization dependency. This is typically characterized by an increase and decrease in EXAFS amplitudes when more or less aligned or perpendicular to the polarization vector ε. For full details, we would like to refer you to van Veelen et al., (2016)[9], and Hudson et al., (1996)[12].

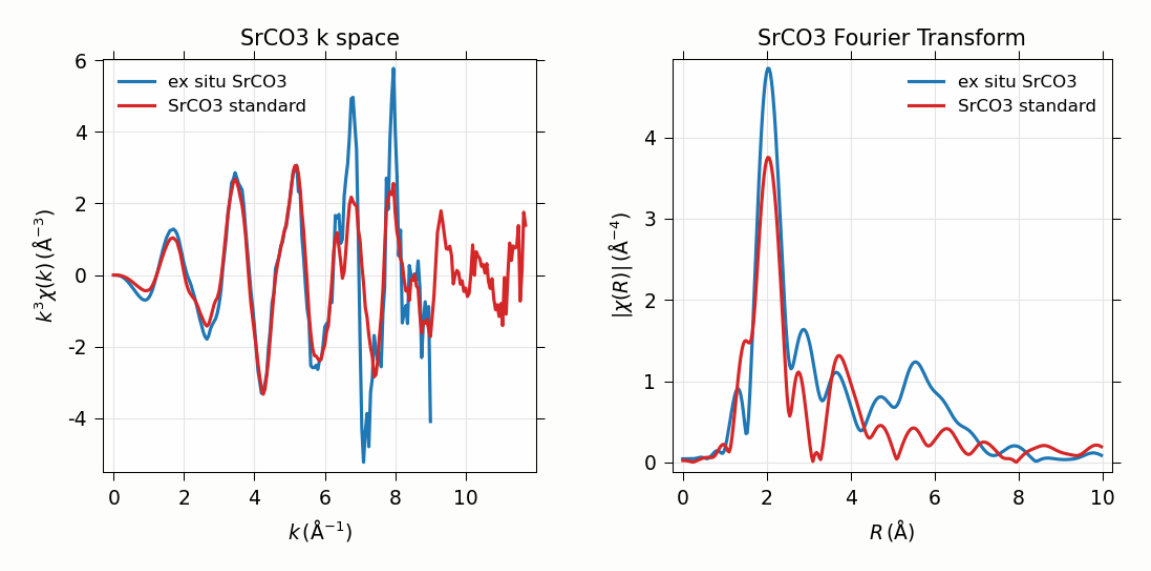

Figure S8. Comparison of powdered $SrCO_3$ standard prepared for fluorescence measurements, and a $SrCO_3$ adsorbate on rutile(110).

Table S6. Fitting parameters of ex situ $SrCO_3$

Shell	CN	R	σ	S_0^2	r-factor
One shell of oxygen – uncorrected					
Sr-O	9	2.63 (2)	0.001 (4)	0.48 (14)	0.10
One shell of oxygen – corrected					
Sr-O	4.8	2.63 (3)	0.001 (2)	0.91 (fixed	0.15
$SrCO_3$ fit –float S_0^2					
Sr-O	9	2.62 (2)	-0.004 (3)	0.40 (8)	0.08
Sr-C	3.8	2.92 (4)	-0.009 (4)		
$SrCO_3$ fit – fix S_0^2 to earlier determined value					
Sr-O	9	2.66 (3)	0.002 (3)	0.91 (fixed)	0.034
Sr-C	3.8	3.07 (4)	0.006 (8)		
$SrCO_3$ fit – fitted S_0^2 to					
Sr-O	9	2.66 (3)	0.010 (1)	1.08	0.021
Sr-C	6	3.09 (3)	0.007 (5)		

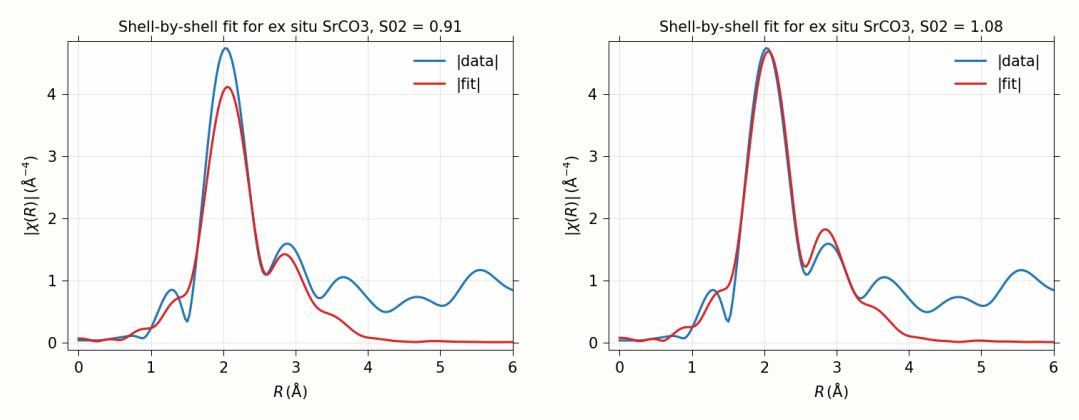

Figure S9. Comparison of *ex situ* $SrCO_3$ sample with selecting S_0^2 determined from the $SrCO_3$ and optimized for a better fit.

By looking at the fits, we can observe that CN number is severely under estimated, due to the polarization dependence. Keeping the coordination reasonable, means that the S_0^2 goes up too.

Further reading:

van Veelen, A., et al. (2016). "Uranium Immobilization and Nanofilm Formation on Magnesium-Rich Minerals." Environmental Science & Technology **50**(7): 3435-3443.

Hudson, E. A., et al. (1996). "Polarized x-ray-absorption spectroscopy of the uranyl ion: Comparison of experiment and theory." Physical Review B **54**(1): 156-165.